# Effects of heat straightening on intergranular corrosion of Al-Zn-Mg alloy

.


## ABSTRACT

The present study aimed to investigate the corrosion resistance of Al-Zn-Mg alloy under different times of heat straightening, utilizing the intergranular corrosion (IGC) and electrochemical testing. The results indicated a decrease in the IGC resistance of the Al-Zn-Mg alloy as a result of heat straightening. The maximum intergranularcorrosion depth of 105 μm was obtained after one time of heat straightening.The discussion on the IGC behavior was centered on changes in precipitation at the grain boundaries and within the matrix. As the heat straightening times increased, the precipitate-free zone (PFZ) disappeared, and the precipitate phases underwent dissolution and re-precipitation. Notably, the sample after one time of heat straightening exhibited the most severe corrosion among the specimens, which was attributed to the higher precipitation coverage rate at the grain boundaries.



*Keywords: heat straightening; intergranular corrosion; electrochemical testing; Al-Zn-Mg alloys*


## 1 INTRODUCTION

"Al-Zn-Mg alloys are widely employed in aerospace industry, rail transit, and military equipment due to their remarkable specific strength and good weldability. Metal inert-gas (MIG) arc welding is commonly used for joining Al-Zn-Mg alloys with Al-Mg filler ER5356 in structural components. However, the high thermal conductivity and thermal expansion coefficient, in comparison to carbon steels, make it prone to welding distortion. This distortion can lead to issues such as dimensional inaccuracies during the assembly and escalated fabrication costs"[1-3]."Therefore, its effective control, especially in large welded structures during assembly, is critical. During the assembly process, it is influenced not only by local shrinkage due to rapid heating and cooling but also by root gap and misalignment between parts to be welded"[1-3]. "Therefore, as its complete elimination is practically challenging, measures need to be taken to reduce it after welding. In this context, here are two primary methods for correcting welding distortion after welding, known as mechanical rectification and heat straightening"[4]. "While mechanical rectification is suitable for small parts, heat straightening is typically employed for larger components, such as blocks and subassemblies. Heat straightening rectifies a metal plate through inflation resulting from localized heating. The characteristics of metal materials, involving heat-expansion-cold-shrinkage, lead to the formation of constringent plastic distortion in the metal plate because the swell is hampered by surrounding colder areas. New constringent plastic distortions counteract the previous distortions as the temperature falls after heating stops"[4]. Despite its widespread use in actual production processes due to low cost and ease of operation [5-8], it is essential to acknowledge that heat straightening can affect the corrosion properties of the workpiece.The heat straightening is a non-isothermal heat treatment (NIHT) process andthe highest temperature for Al-Zn-Mg alloys usually reaches 400 °C,then the parameters in precipitation process, including diffusion,driving force and nucleation barriers, evolve simultaneously.

"Al-Zn-Mg alloys are often susceptible to localized corrosion, particularly along grain boundaries, such as IGC, exfoliation corrosion (EXCO) and stress corrosion cracking (SCC). The consensus is that the microstructure and microchemistry at grain boundaries play a pivotal role in the low resistance to localized corrosion of these alloys. In order to enhance the corrosion resistance of Al-Zn-Mg alloys, various investigations have been conducted to modify the grain boundary microstructure, including the composition and morphology of

precipitates at grain boundaries. Over-aging (T7x) or retrogression and re-aging (RRA) significantly reduce the corrosion susceptibility of Al-Zn-Mg alloys”[9-11]. “The over-aging treatment (T7x) can enhance the corrosion resistance but comes with a loss of about 10-15% in strength”[12]. “Compared toT7x temper, RRA can achieve high strength and high corrosion resistance. However, it poses technical challenges for thick plate production due to the relatively short retrogression process in RRA temper, ranging from a few seconds to an hour or so”[13]. “Therefore, to address the corrosion susceptibility of Al-Zn-Mgalloys, alternative treatments have been proposed. Ou et al. introduced a step-quench and aging (SQA) treatment to improve both the strength and corrosion resistance of the 7050 aluminum alloy”[14]. Huang et al. reported “a high temperature pre-precipitation(HTPP) treatment”[15, 16]. The goal of these treatments was to obtain coarse and distributed discontinuous grain boundary precipitates, which are beneficial for enhancing the corrosion resistance.

While numerous studies have focused on different aging treatments, such as peak aging (T6), over-aging (T7x),retrogression and re-aging (RRA) of aluminum alloys, few have reported T5 condition in recent decades. The T5 condition is defined as the state of an aluminum alloy that is cooled in high-temperature molding process and then artificially aged. In recent years, extrusion profiles of Al-Zn-Mg alloys in the T5 condition have become widely used in rail transit.In thepresent study, Al-Zn-Mg alloys were supplied in the T5 condition, aiming to understand the effect of heat straightening on their corrosion susceptibility based on IGC and electrochemical testingas well as microstructure characterization by transmission electron microscopy (TEM).

The objective was to identify the mechanism leading to the decrease in corrosion resistance and then to improve the heat straightening technologyapplied to Al-Zn-Mg alloys.

## 2 METHOD

The base material used in the present study was a 10-mm thick extruded Al-Zn-Mg alloy platesupplied in T5 condition, as shown in Fig. 1. Table 1 shows chemical composition of this alloy. Table 2 details its basic mechanical and electrical properties. The samples of as-received Al-Zn-Mg alloy were heated to $400\pm10^{o}$Cfor different times using oxygen-propane flame, as outlined in Table 3. The temperature of samples was monitored using Tempilstic temperature pen (TS0400), and the torch was moved at a constant speed around the heated area to ensure a uniform temperature distribution. Following the heat straightening process, the samples were promptly quenched using water. In the actual correction process, due to variations in welding deformations, frequently conduct multiple heat straightening, with the number of heat straightening typically not exceeding three. Consequently, the samples were heated for different numbers of times (once, twice, triple) by repeating the previously mentioned heating and quenchingprocess to compare with those without heat treatment, as listed in Table 3.

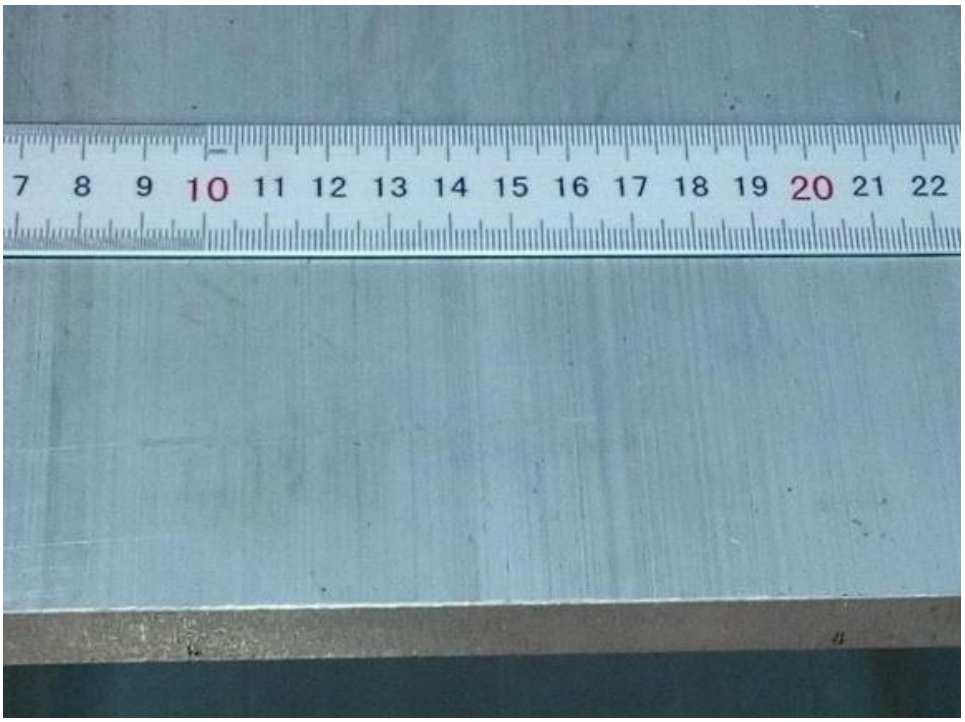


Fig.1. Macro-appearance ofas-received Al-Zn-Mgalloy.

Table 1.Chemical composition of as-received Al-Zn-Mg alloy (wt.%)

| Zn | Mg | Mn | Cr | Zr | Fe | Cu | Ti | Si | V | Al |
|---|---|---|---|---|---|---|---|---|---|---|
| 4.480 | 1.547 | 0.294 | 0.232 | 0.180 | 0.125 | 0.113 | 0.054 | 0.050 | 0.014 | Bal. |

Table 2Basic mechanical and electrical properties of as-received Al-Zn-Mg alloy

| Tensile strength (MPa) | Yield strength (MPa) | Elongation (%) | Hardness (HV) | Conductivity (%IACS) |
|---|---|---|---|---|
| 360 | 295 | 20.6 | 104.3 | 36.5 |

Table 3 Heating parameters of Al-Zn-Mg alloy

| Samples No. | Temperature($^{o}$C) | Rectification times |
|---|---|---|
| FR0 | - | - |
| FR1 | 400 | One time |
| FR2 | 400 | Two times |
| FR3 | 400 | Three times |

Specimens measuring 40 mm×25 mm×8 mm were prepared for IGCtesting, according to recommendations of the Chinese National StandardGB/T 7998-2005[17]. The testing was conducted in a water bath in a solution of 1.0 mol/L NaCl + 0.01 mol/L $H_2O_2$. The solution temperature was set at 35±2$^{o}$C, while testing time was 6h. The ratio of the metal surface to the solution volume was less than 20 mm$^2$/mL. Prior to testing, the samples were ground to 1200 grit (SiC paper) and degreased with acetone. Subsequently, the cross-sectional corrosion appearance and corrosion depth were examined using an optical microscope (OM). The statistics on the corrosion depth values was obtained from 3 repeated IGC tests at different locations in the case of each sample. The maximum corrosion depth was used to compare the IGC resistance of different heat-treated samples.

Potentiodynamic polarization experiment and electrochemical impedance spectroscopy (EIS) testing, known for estimating the resistance to IGC of aluminum alloy [9, 18-20], were

also employed in the present study. Potentiodynamic polarization measurements were carried out using a CHI660E Electrochemical Workstation and an electrochemical cell with a three-electrode arrangement. The three-electrode system comprised a saturated calomel electrode (SCE) as the reference electrode, a large platinum sheet as the counter electrode, and the studied alloy as the working electrode. The potentiodynamic polarization experiments were performed immediately after the Open Circuit Potential (OCP) tests. The procedure involved starting at -300 mV (relative to OCP) and then polarizing to +300 mV (relative to OCP) at a scan speed of 10 $mVs^{-1}$. Tafel-type fitting of the data was performed to estimate the self-corrosion potential ($E_{corr}$) and corrosion rate ($i_{corr}$) from the polarization curves using CorrView software. EIS testing was carried out at the OCP with the frequency ranging from 0.01 Hz to 10 kHz using a 5 mV AC signal. All tests were conducted at room temperature in 3.5 wt.% NaCl solution, whereas the exposed surface area was 1 $cm^2$.

For microstructural examination, samples were sectioned from the plates. After grinding and polishing, samples were made into foils with 100 μm in thickness, which was followed by the double electro-polishing in the solution of 25 vol.% $HNO_3$ + 75 vol.% $CH_3OH$ at -25$^oC$for examination under TEM.

# 3 RESULTS

## 3.1 IGC testing

Fig. 2 shows the results of immersion corrosion testing of samples that were subjected to different times of heat straightening. The maximum corrosion depth of samples varied significantly with different times of heat straightening. The IGC morphology typically exhibited a combination of pitting and network structure characteristic. Table 4 provides an overview of the evolution of the IGC tests for samples with different times of heat straightening. For sample FR0, no evident corrosion characteristics were detected, and the maximum corrosion depth was less than 10 μm, as shown in Fig. 2(a). In contrast, a severe IGC feature is evident in Fig. 2(b) for sample FR1, with the maximum corrosion depth of 105 μm. The corrosion depth of specimen FR2, after 6 h of immersion, decreased from 105 μm with one time of heat straightening to 60 μm with two times of heat straightening, as shown in Fig. 2(c).Sample FR3 exhibited a higher IGC susceptibility compared to FR2 sample. Based on these results, it is reasonable to conclude that the maximum corrosion depth was greatest for specimen FR1, with the ranking in the following order: FR1＞FR3＞FR2＞FR0. A larger corrosion depth indicated lower corrosion resistance. It is evident that the corrosion resistance of the Al-Zn-Mg alloy was reduced to varying extents with different times of heat straightening.

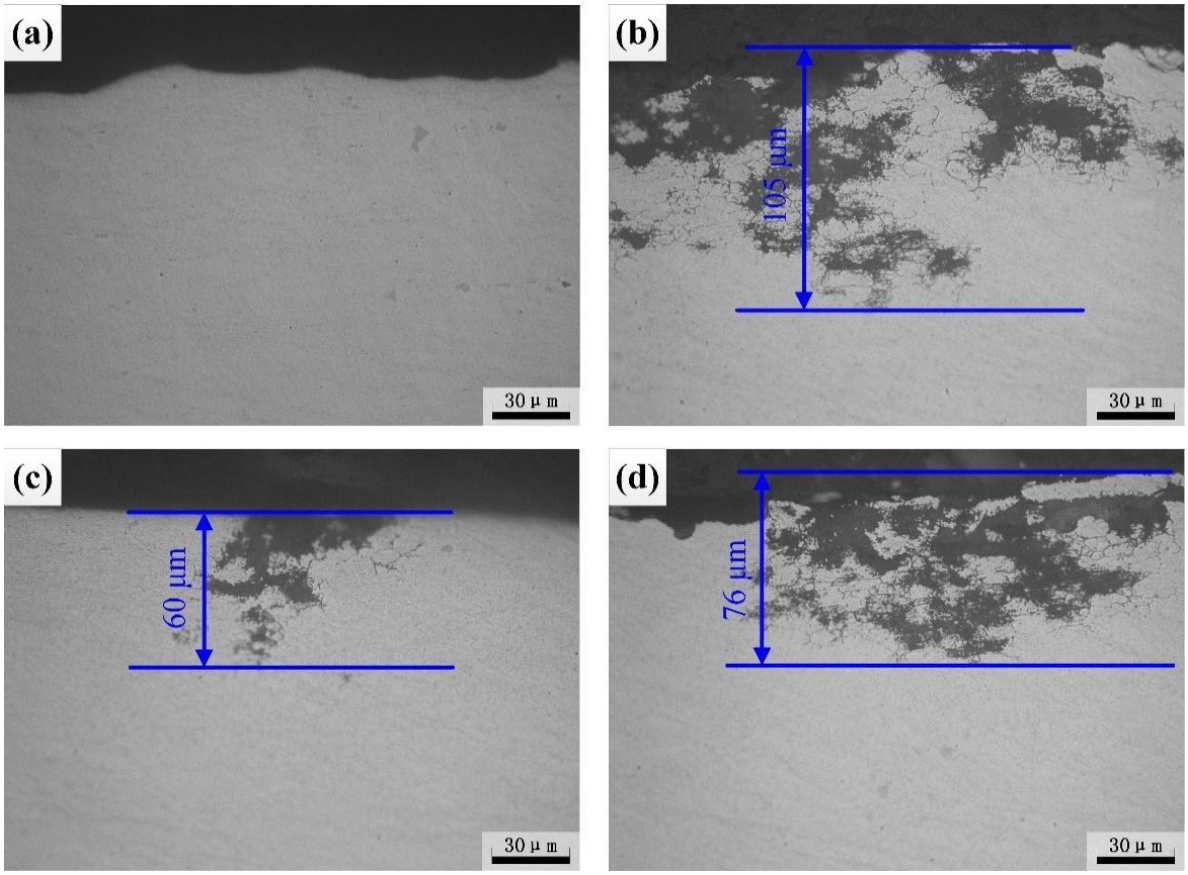


Fig. 2. Metallographic micrographs after IGC testing of (a) base metal and samples after (b) one time, (c) two times, and (d) three times of heat straightening at 400$^{o}$C.

Table 4. The evolution of maximum corrosion depth for samples with different times of heat straightening.

| Samples No. | Rectification times | Maximum depth(μm) |
|---|---|---|
| FR0 | - | <10 |
| FR1 | One time | 105 |
| FR2 | Two times | 60 |
| FR3 | Three times | 76 |

**3.2 Electrochemical testing**

The typical polarization curves presented in Fig.3 illustrate notable variations in both the corrosion potential*E*corrand anodic polarization behavior between sample FR0 and those subjected to different times of heat straightening. The *E*corr values shifted towards the nobler direction after heat straightening. However, the shape of the cathodic portion of these curves remained essentially unchanged with different times of heat straightening. The log current density increased linearly with potential above 60 mV relative to the corrosion potential *E*corr, approaching Tafel-type behavior, although the anodic portion showed some passivation characteristic. The corrosion rate ($i_{corr}$) was calculated by Tafel extrapolation using CorrView software, and the corresponding results are listed in Table5. The corrosion rate ($i_{corr}$) of studied samples increased after heat straightening, aligning with the results of IGC tests. This suggested that the Tafel method was suitable for determining the corrosion rate($i_{corr}$)of samples, although the fitting process may be subjective.

To delve deeper into the electrochemical response of alloys subjected to different times of heat straightening, the EIS testing was carried out. The typical Nyquist plots of the samples undergoing different times of heat straightening are displayed in Fig. 4(a). The

corrosion resistance of specimens demonstrated a positive correlation with the radius of capacitive reactance arc. It is evident that this radius for sample FR0 was largest and followed the order: FR0＞FR2＞FR3＞FR1. The EIS results indicated that heat straightening at 400$^{o}$C deteriorated the corrosion properties of the Al-Zn-Mg alloy, especially after one time of heat straightening. “The equivalent circuit model in Fig. 4(b) was used to analyze the experimental data using ZView software, and the results are listed in Table 6. The charge transfer resistance (*R*t), which indicates corrosion rate, was analyzed. Of all samples, the *R*t value was the highest in the case of sample FR0, with the maximum *R*t value of 10820 Ω·cm$^2$, and the lowest in the case of sample FR1, with a numerical value of 1341Ω·cm$^2$. A higher *R*t value corresponds to a lower corrosion current density and, consequently, better corrosion resistance”[18, 21]. Based on the results of electrochemical testing, it is reasonable to conclude that heat straightening led to a decrease in the corrosion resistance of samples.

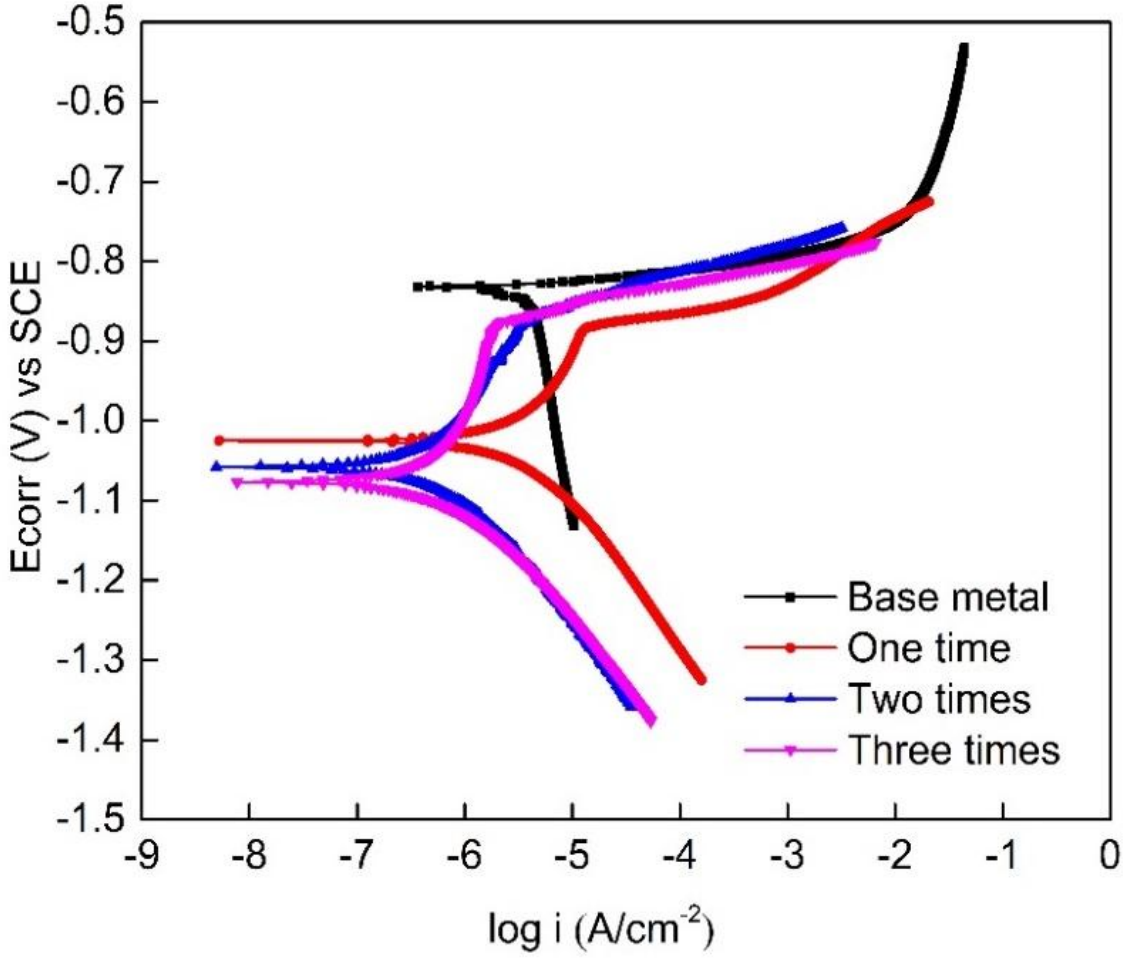


Fig. 3. Polarization curves of samples with different times of heat straightening.

Table 5. Electrochemical parameters obtained from the polarization plots.

| Samples No. | Rectification times | $E_{corr}$(V) vs SCE | $i_{corr}$(A/cm$^{-2}$) |
|---|---|---|---|
| FR0 | - | -0.832 | 3.2E$^{-7}$ |
| FR1 | One time | -1.025 | 4.0E$^{-6}$ |
| FR2 | Two times | -1.058 | 6.5E$^{-7}$ |
| FR3 | Three times | -1.070 | 5.3E$^{-7}$ |

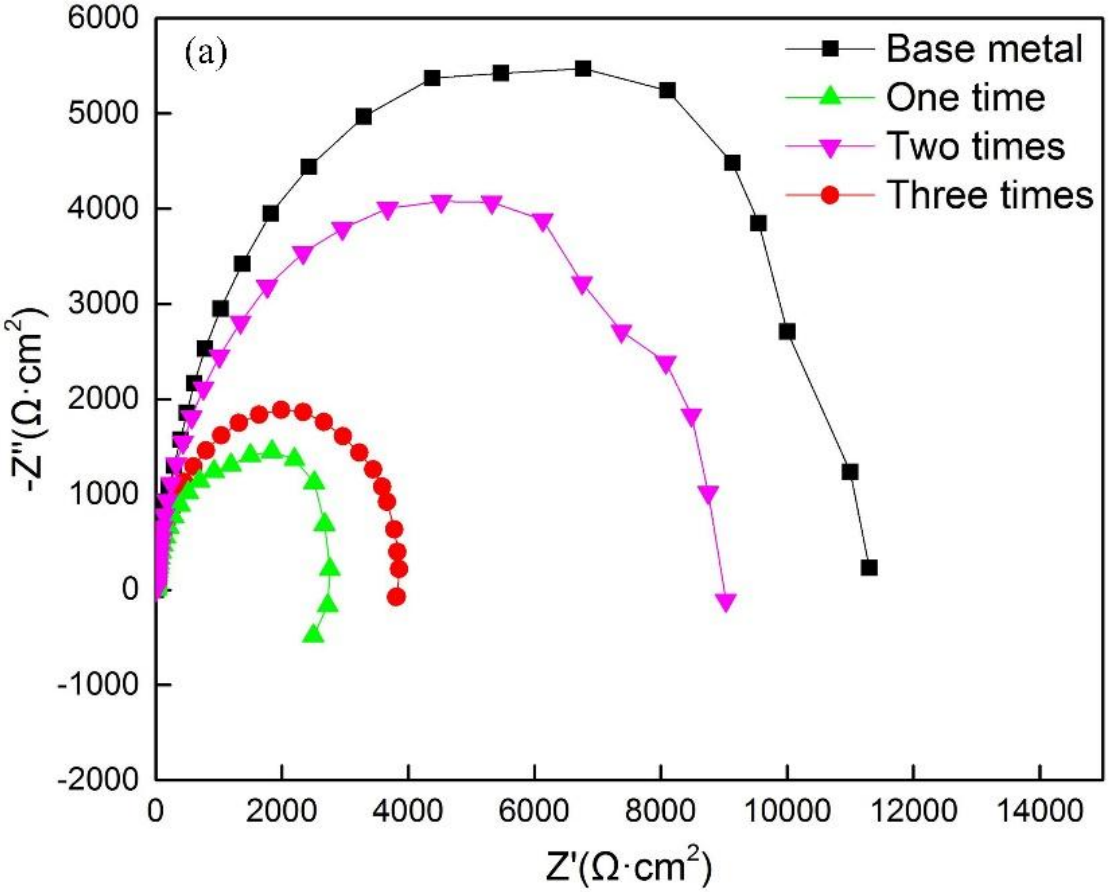


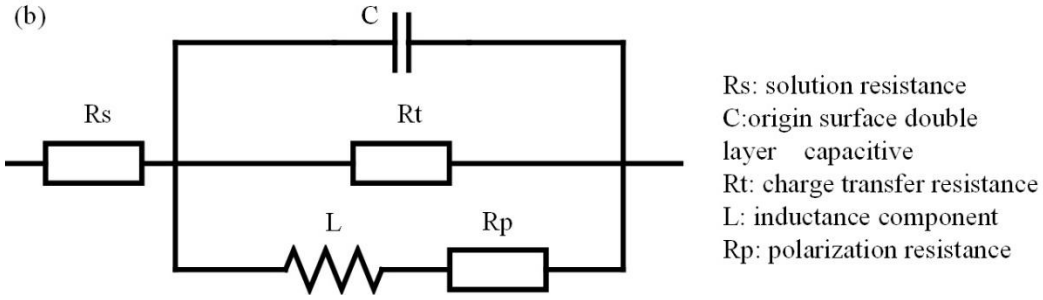


Fig. 4. Effect of heat straightening times on the impedance spectra of specimens after immersion in 3.5 wt.% NaCl solution. (a) Nyquist plots and (b) equivalent circuit used to simulate the corrosion behavior of specimens immersed in the solution.

Table 6. Electrochemical parameters obtained from the polarization plots.

| Samples No. | Rectification times | Rs/Ω·cm$^2$ | C/μF·cm$^{-2}$ | Rt/Ω·cm$^2$ | L/μH·cm$^{-2}$ | Rp/Ω·cm$^2$ |
|---|---|---|---|---|---|---|
| FR0 | - | 6.533 | 9.543 | 10820 | 4627 | 1664 |
| FR1 | One time | 1.590 | 15.95 | 1341 | 3732 | 317.4 |
| FR2 | Two times | 1.518 | 5.009 | 2570 | 599.4 | 451.8 |
| FR3 | Three times | 3.952 | 9.966 | 7949 | 31320 | 2014 |

**3.3 Grain boundary microstructure**

During the heat straightening, various microstructural transformations are likely to occur, such as recrystallization, grain growth, and modification of precipitates [22]. The last involves processes such as the dissolution of precipitates, growth of precipitates, and their

transformation from coherent into incoherent forms. The manifestation of IGC primarily occurs along the grain boundaries, and the transformation in corrosion resistance is closely linked to the evolution of the grain boundary precipitates [23]. Therefore, attention was focused on the transformation in grain boundary microstructure after heat straightening. Fig. 5 presents the typical TEM microstructures near grain boundaries in samples treated with different times of heat straightening. As shown in Fig. 5(a), the extruded Al-Zn-Mg alloy plate in the T5 condition mainly contained discrete precipitates in grain boundaries and G.P. (Guinier-Preston) zones, along with the non-equilibrium phase η′ in Al matrix. Simultaneously, there was a PFZ near the grain boundary precipitates, which was less than 30 nm on each side of the boundary. To clarify category of precipitate phases, a selected area diffraction pattern (SADP) in the Al<112> projection from sample FR0 was obtained, as shown in Fig. 6. The main strong diffraction spots originated from the Al matrix.SADP analysis indicated that the extra diffraction spots mainly resulted from the η′ phase and η phase,contributing to the strength of Al alloys [24]. After heat straightening, the precipitations in samples, especially the matrix precipitates (MPt), underwent noticeable changes. In sample FR1, most of the MPts dissolved into the matrix and some MPts grew. The grain boundary precipitates became continuous and coarser, as depicted in Fig. 5(b), which was detrimental to the corrosion resistance of aluminum alloys[9-11]. In Fig. 5(c), there were almost no precipitate phases in the Al alloy matrix and along the grain boundary. After three times of heat straightening, the grain boundary precipitates reappeared, as shown in Fig. 5(d), and some sporadic precipitates formed in the matrix. In summary, the precipitates phases of the alloys experienced dissolution and re-precipitation with an increase in times of heat straightening.

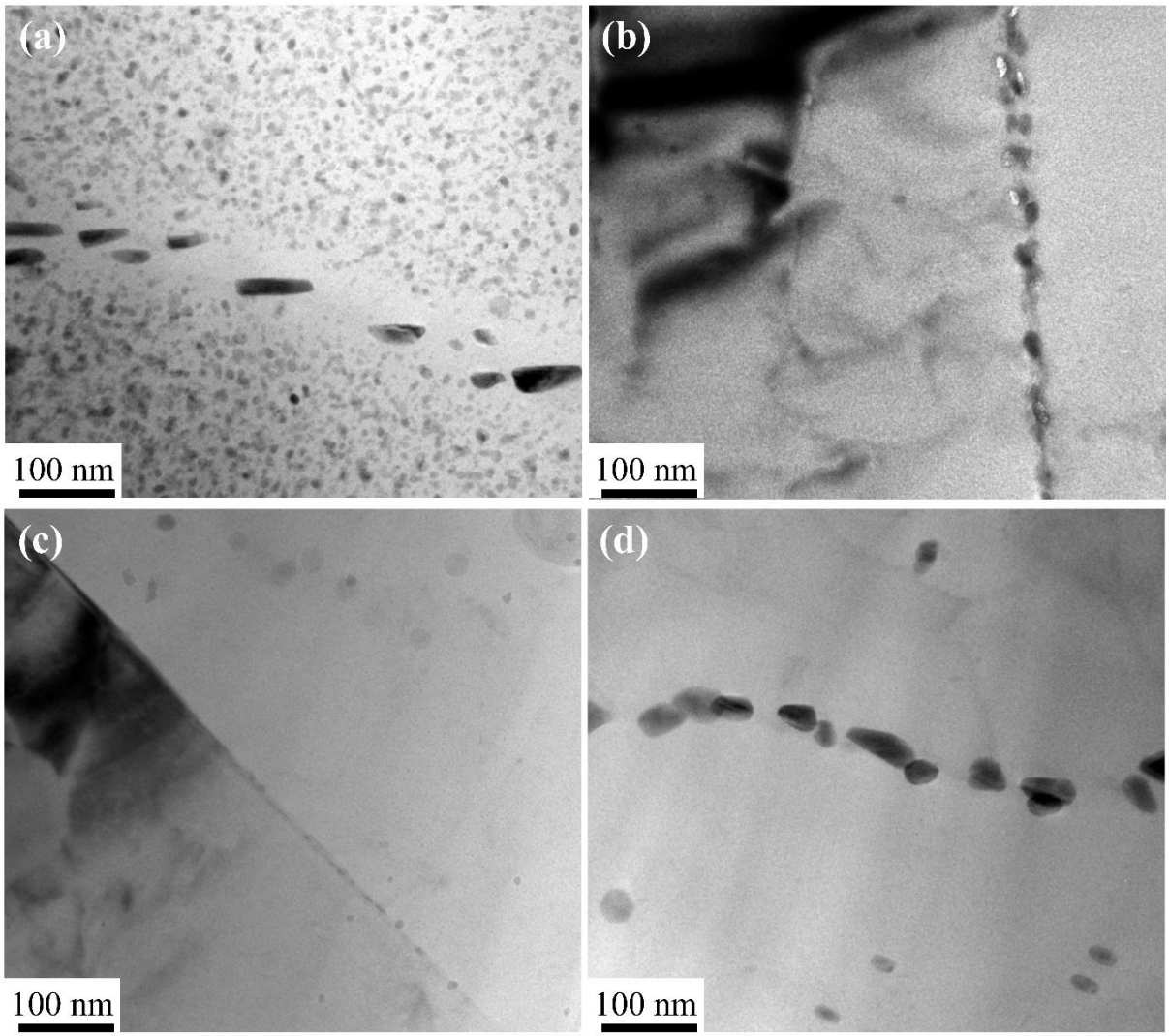


Fig. 5. Grain boundaries of (a) base metal and the samples after (b) one time, (c) two times, and (d) three times of heat straightening at 400$^{o}$C.

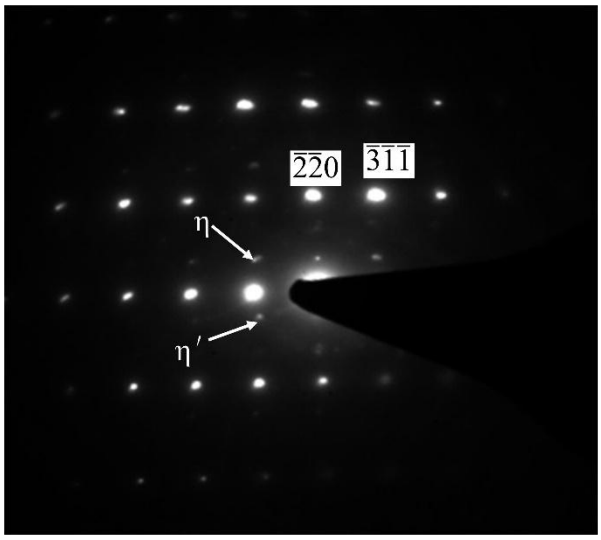


Fig. 6. SAD pattern of the base metal,<112>$_{Al}$ projection

## 4 DISCUSSION

When subjected to different times of heat straightening, the transformation of precipitation depends on the heating rate and the characteristics of the initially present precipitates. Schematically, in typical 7000 alloys, the dissolution of phases occurs in the range of 50-150$^{o}$C for G.P. zones, 200-250$^{o}$C for η′ precipitations, and 300-350$^{o}$C for η precipitations [25, 26].From the results of IGC and electrochemical testing, the IGC resistance of Al-Zn-Mg alloy decreased after heat straightening. As IGC occurred along grain boundaries, it is reasonable to assume that the change in corrosion resistance was related to the transformation of microstructure in the grain boundary. As shown in Fig.5, the microstructure of samples varied significantly after different times of heat straightening. After one time of heat straightening at 400$^{o}$C, the dominant phenomenon was the dissolution of the initial matrix precipitates (G.P. zones, η′ and η phase) with dimensions less than the critical dimension. Other precipitates, with dimensions larger than the critical dimension, grew.Simultaneously, the grain boundary precipitates became coarser and continuous, as shown in Fig. 5(b). In Fig. 5(c), with an increase of times of heat straightening, the precipitate phases continued to dissolveduring the heating process of the second heat straightening and formed super-saturated solid solution. However, there wasonly some elements segregation and no significant precipitations at the grain boundariesbecause the super-saturated degree was low. “After theheating process of the third heat straightening, the increase in the super-saturated degree of the alloy allowed some solute atoms to be used for the precipitation of η at grain boundaries during the quenching process. In the aging process, the precipitation relies more on the kinetics of the procedure. If the alloy matrix is at a low super-saturated solution degree, the precipitation in the grain and at the grain boundary is primarily controlled by thermodynamics”[27]. “Precipitation can occur during the cooling down process at a high temperature. Additionally, the well-known tendency for preferable precipitation in the grain boundary is very apparent for Al-Zn-Mg alloys”[28]. Consequently, after three times of heat straightening, a few η phase particles were preferentially precipitated at the grain boundaries.

“According to the anodic dissolution mechanism, the driving force for the corrosion of Al-Zn-Mg alloy is the potential difference between the grain boundary precipitates η ($MgZn_2$) and the matrix”[12, 29, 30]. “The η phase always acts as the anode, while the PFZ and matrix act as the cathode. In solutions containing $Cl^-$ ions, numerous corrosion micro-cells can form in the corrosive solution due to potential differences [26, 28]. The preferential dissolution of anodic phases (η phase) in the cells leads to the formation of anodic dissolution paths at grain boundaries, ultimately inducing intergranular corrosion. The

coverage rate of precipitates at grain boundaries in sample FR1 was higher than in the other samples. Therefore, sample FR1 was the most severely corroded in this test"[31-33]. For sample FR2, nearly all the precipitations dissolved into the matrix, and the potential difference between the grain boundary and matrix decreased, reducing the degree of corrosion. With an increase of times of heat straightening, the η phases re-precipitated at grain boundaries, so the potential difference increased and the degree of corrosion increased.

## 5 CONCLUSIONS

The corrosion resistance of Al-Zn-Mg alloy subjected to different times of heat straightening at 400$^{o}$C was investigated through IGC and electrochemical testing. After one time of heat straightening, transformation of precipitation in the alloy caused formation of high coverage rate of precipitates at the grain boundaries, increased the potential difference between the grain boundary precipitates η and the matrix, resulting in the most severe corrosion. The precipitation in the alloy continued to dissolve after two times of heat straightening, forming a super-saturated solid solution. Consequently, the potential difference between the grain boundary and matrix decreased, reducing the degree of corrosion. After thethird heat straightening, the increase in the super-saturated degree of the alloy allowed some solute atoms be used for the precipitation of □ at the grain boundaries.A few stable phases preferentially precipitated at the grain boundaries during the quenching process, subsequently increasing the potential difference and the corrosion degree. After different times of heat straightening, the precipitate-free zone disappeared and the aluminum alloy experienced dissolution and re-precipitation.


## ACKNOWLEDGEMENTS

This research was supported by the Henan Province Science and Technology Research Project (No.232102220055).


## COMPETING INTERESTS

There is no conflicts of interest for this research paper

## AUTHORS' CONTRIBUTIONS

Shuai Li and Jiyuan Ding: Performed the experiments and write the manuscript; Dejun Yan Contributed to the conception and design of the study; GuoshunYang and Rongzheng Xu: Helped perform the analysis with constructive discussions; Chuanqing Liao and Tingting Wu: Played an important role in interpreting the results; Yonggang Jiang:contributed to the conception and design of the study. All authors read and approved the final manuscript.All authors have read and agreed to the published version of the manuscript.

## REFERENCES


[1] D. Deng, FEM prediction of welding residual stress and distortion in carbon steel considering phase transformation effects, Mater. Design, 30 (2009) 359-366.

[2] D. Deng, H. Murakawa, Prediction of welding distortion and residual stress in a thin plate butt-welded joint, Comp. Mater. Sci., 43 (2008) 353-365.

[3] D. Deng, H. Murakawa, W. Liang, Numerical simulation of welding distortion in large structures, Comput Method. Appl. M., 196 (2007) 4613-4627.

[4] Z. Zhang, Z. Jiang, C. Yu, Automated flame rectification process planning system in shipbuilding based on artificial intelligence, Int. J. Adv. Manuf. Tech., 30 (2006) 1119-1125.

[5] A. Cullison, Engineer Provides Flame Straightening Techniques, Weld. J. 74 (1995) 12-12.

[6] F. Hanus, R. Hubo, Flame straightening of thermomechanically rolled structural steel, Steel Res., 70 (1999) 193-197.

[7] R. Hubo, D. Kugler, J. Petersen, H. Wegmann, Influence of Flame Straightening on the Properties of Thermomechanically Rolled Shipbuilding Steels, Stahl. Eisen., 114 (1994) 97-99.

[8] B.K. Vackar, R.J. Dolida, Effect of Flame Straightening Heat on Austenitic Stainless-Steel, Weld. J., 60 (1981) 25-27.

[9] G.S Peng, K.H. Chen, S.Y. Chen, H.C. Fang, Influence of dual retrogression and re-aging temper on microstructure, strength and exfoliation corrosion behavior of Al-Zn-Mg-Cu alloy, T. Nonferr. Metal. Soc., 22 (2012) 803-809.
[10] J.F. Li, N. Birbilis, C.X. Li, Z.Q. Jia, B. Cai, Z.Q. Zheng, Influence of retrogression temperature and time on the mechanical properties and exfoliation corrosion behavior of aluminium alloy AA7150, Mater. Charact., 60 (2009) 1334-1341.
[11] F. Andreatta, H. Terryn, J.H.W. de Wit, Corrosion behaviour of different tempers of AA7075 aluminium alloy, Electrochim. Acta., 49 (2004) 2851-2862.
[12] Y. Deng, Z. Yin, K. Zhao, J. Duan, J. Hu, Z. He, Effects of Sc and Zr microalloying additions and aging time at 120°C on the corrosion behaviour of an Al-Zn-Mg alloy, Corros. Sci., 65 (2012) 288-298.
[13] A.F. Oliveira, M.C. de Barros, K.R. Cardoso, D.N. Travessa, The effect of RRA on the strength and SCC resistance on AA7050 and AA7150 aluminium alloys, Mat. Sci. Eng. A-Struct., 379 (2004) 321-326.
[14] B.L. Ou, J.G. Yang, M.Y. Wei, Effect of homogenization and aging treatment on mechanical properties and stress-corrosion cracking of 7050 alloys, Metall. Mater. Trans. A, 38A (2007) 1760-1773.
[15] L. Huang, K. Chen, S. Li, Influence of grain-boundary pre-precipitation and corrosion characteristics of inter-granular phases on corrosion behaviors of an Al-Zn-Mg-Cu alloy, Mater. Sci. Eng. B-Adv., 177 (2012) 862-868.
[16] L.P. Huang, K.H. Chen, S. Li, M. Song, Influence of high-temperature pre-precipitation on local corrosion behaviors of Al-Zn-Mg alloy, Scripta Mater., 56 (2007) 305-308.
[17] GB/T 7998-2005, Test method for intergranular corrosion of aluminium alloy, 2005.Chinese.
[18] F.H. Cao, Z. Zhang, J.F. Li, Y.L. Cheng, J.Q. Zhang, C.N. Cao, Exfoliation corrosion of aluminum alloy AA7075 examined by electrochemical impedance spectroscopy, Mater. Corros., 55 (2004) 18-23.
[19] A. Conde, J. de Damborenea, Electrochemical modelling of exfoliation corrosion behaviour of 8090 alloy, Electrochim. Acta., 43 (1998) 849-860.
[20] J.F. Li, Z.W. Peng, C.X. Li, Z.Q. Jia, W.J. Chen, Z.Q. Zheng, Mechanical properties, corrosion behaviors and microstructures of 7075 aluminium alloy with various aging treatments, T. Nonferr. Metal. Soc., 18 (2008) 755-762.
[21] M. Keddam, C. Kuntz, H. Takenouti, D. Schuster, D. Zuili, Exfoliation corrosion of aluminium alloys examined by electrode impedance, Electrochim. Acta., 42 (1997) 87-97.
[22] S.Li,H.G.Dong,L. Shi,P. Li, F. Ye. Corrosion behavior and mechanical properties of Al-Zn-Mg aluminum alloy weld, Corros. Sci.123(2017)243-255.
[23] S.Li,H.G.Dong,P. Li, S.Chen. Effect of repetitious non-isothermal heat treatment on corrosion behavior of Al-Zn-Mg alloy, Corros. Sci.123(2018)278-289.
[24] G. Sha, A. Cerezo, Early-stage precipitation in Al-Zn-Mg-Cu alloy (7050), Acta. Mater., 52 (2004) 4503-4516.
[25] L.B. Ber, Accelerated artificial ageing regimes of commercial aluminium alloys. II: Al-Cu, Al-Zn-Mg-(Cu), Al-Mg-Si-(Cu) alloys, Mat. Sci. Eng. A-Struct., 280 (2000) 91-96.
[26] S.Li,H.G.Dong, X.X. Wang, Z.Y. Liu, Z.J. Tan, L.J.Shangguan. Effect of repair welding on microstructure and mechanical properties of7N01 aluminum alloy MIG welded joint, J Manuf. Process.,54(2020)80-88.
[27] P. Guyot, L.Cottignies, Precipitation kinetics, mechanical strength and electrical conductivity of AlZnMgCu alloys, Acta. Mater., 44 (1996) 4161-4167.
[28] Y.F. Jiang, S.Y.Xu, S. Gao. The effect of initial alloy temper on corrosion resistance for Al-Zn-Mg-Cu alloy, Corros. Sci.209(2022)1170730.
[29] B.S.Han, X. Zheng, W. wang, Y. Zhang, Y.J. Xu, K.Z. He, Y.S. Zeng, X.M. Zhang. Microstructures and properties of a high strength, toughness, and corrosion resistance Al-Zn-Mg-Cu alloy under an over-aging state, Mater. Lett., 325(2022)132674.

[30] D. Zhang, H.C. Jiang, Z.J. Cui, D.S. Yan, Y.Y. Song , L.J. Rong.Synchronous improvement of mechanical properties and stress corrosion resistance by stress-aging coupled with natural aging pre-treatment in an Al-Zn-Mg alloy with high recrystallization fraction,J. Mater. Sci. Technol.,121(2022)40-51.
[31] S.P. Knight, N. Birbilis, B.C. Muddle, A.R. Trueman, S.P. Lynch, Correlations between intergranular stress corrosion cracking, grain-boundary microchemistry, and grain-boundary electrochemistry for Al-Zn-Mg-Cu alloys, Corros. Sci., 52 (2010) 4073-4080.
[32] S.D. Liu, B. Chen, C.B. Li, Y. Dai, Y.L. Deng, X.M. Zhang, Mechanism of low exfoliation corrosion resistance due to slow quenching in high strength aluminium alloy, Corros. Sci., 91 (2015) 203-212.
[33] F. Song, X. Zhang, S. Liu, Q. Tan, D. Li, The effect of quench rate and overageing temper on the corrosion behaviour of AA7050, Corros. Sci., 78 (2014) 276-286.

364